Acta Oceanol. Sin., 2024, Vol. 43, No. 7, P. 125–137
https://doi.org/10.1007/s13131-024-2384-x
http://www.aosocean.com
E-mail: ocean2@hyxb.org.cn

A bulk extraction method to determine the stable isotope ratios of iron, nickel, copper, zinc, and cadmium in seawater using multi-collector inductively coupled plasma mass spectrometry

Zhan Shen[1], Yuncong Ge[1], Jiahui Liu[1], Wenkai Guan[1], Wenfeng Hu[2], Ruifeng Zhang[1, 3, 4, 5*]

[1] School of Oceanography, Shanghai Jiao Tong University, Shanghai 200030, China

[2] Southern Marine Science and Engineering Guangdong Laboratory (Zhuhai), Zhuhai 519015, China

[3] Shanghai Key Laboratory of Polar Life and Environment Sciences, Shanghai Jiao Tong University, Shanghai 200030, China

[4] Key Laboratory of Polar Ecosystem and Climate Change of Ministry of Education, Shanghai Jiao Tong University, Shanghai 200030, China

[5] Laboratory for Polar Science, Polar Research Institute of China, Ministry of Natural Resources, Shanghai 200136, China

Received 13 January 2024; accepted 7 March 2024

Abstract

The oceanic trace metals iron (Fe), nickel (Ni), copper (Cu), zinc (Zn), and cadmium (Cd) are crucial to marine phytoplankton growth and global carbon cycle, and the analysis of their stable isotopes can provide valuable insights into their biogeochemical cycles within the ocean. However, the simultaneous isotopic analysis of multiple elements present in seawater is challenging because of their low concentrations, limited volumes of the test samples, and high salt matrix. In this study, we present the novel method developed for the simultaneous analysis of five isotope systems by 1 L seawater sample. In the developed method, the NOBIAS Chelate-PA1 resin was used to extract metals from seawater, the AG MP-1M anion-exchange resin to purify Cu, Fe, Zn, Cd, and the NOBIAS Chelate-PA1 resin to further extract Ni from the matrix elements. Finally, a multi-collector inductively coupled plasma mass spectroscope (MC-ICPMS) was employed for the isotopic measurements using a double-spike technique or sample-standard bracketing combined with internal normalization. This method exhibited low total procedural blanks (0.04 pg, 0.04 pg, 0.21 pg, 0.15 pg, and 3 pg for Ni, Cu, Fe, Zn, and Cd, respectively) and high extraction efficiencies (100.5% ± 0.3%, 100.2% ± 0.5%, 97.8% ± 1.4%, 99.9% ± 0.8%, and 100.1% ± 0.2% for Ni, Cu, Fe, Zn, and Cd, respectively). The external errors and external precisions of this method could be considered negligible. The proposed method was further tested on the seawater samples obtained from the whole vertical profile of a water column during the Chinese GEOTRACES GP09 cruise in the Northwest Pacific, and the results showed good agreement with previous related data. This innovative method will contribute to the advancement of isotope research and enhance our understanding of the marine biogeochemical cycling of Fe, Ni, Cu, Zn, and Cd.

Key words: trace metal, stable isotopes, seawater, bulk extraction

Citation: Shen Zhan, Ge Yuncong, Liu Jiahui, Guan Wenkai, Hu Wenfeng, Zhang Ruifeng. 2024. A bulk extraction method to determine the stable isotope ratios of iron, nickel, copper, zinc, and cadmium in seawater using multi-collector inductively coupled plasma mass spectrometry. Acta Oceanologica Sinica, 43(7): 125–137, doi: 10.1007/s13131-024-2384-x

1 Introduction

Iron (Fe), nickel (Ni), copper (Cu), zinc (Zn), and cadmium (Cd), the trace metals essential for marine organisms, have a significant influence on the oceanic biogeochemical cycles (Morel and Price, 2003). These metals in their dissolved phases exhibit nutrient-like vertical profiles. They are taken up in surface waters and subsequently released into deep waters through biogenic particle decomposition. Over the past decades, numerous studies along with the GEOTRACES program (an international study of the marine biogeochemical cycles of trace elements and their isotopes) have extensively examined the oceanic distributions of various elements (SCOR Working Group, 2007; Tagliabue et al., 2017; Weber et al., 2018; Roshan et al., 2018; Middag et al., 2018; Richon and Tagliabue, 2019; John et al., 2022). Dissolved Fe concentrations as low as 0.02 nmol/kg in surface waters can limit oceanic primary productivity, thereby affecting the global carbon cycle and climate change (Boyd and Ellwood, 2010; Falkowski et al., 1998; Morel and Price, 2003). Zn is the second most abundant micronutrient in phytoplankton biomass (Twining and Baines, 2013). Meanwhile Ni plays a crucial role in various biogeochemical processes, including nitrogen and carbon fixation, nitrogen uptake by plants, and methanogenesis (Alfano and Cavazza, 2020). Depending on their concentrations, both Cd and Cu can function as the nutrients or toxins of phytoplankton (Price and Morel, 1990; Payne and Price, 1999; Lane and Morel, 2000).

The concentrations of oceanic trace elements cannot fully

Foundation item: The National Key Research and Development Program of China under contract No. 2022YFE0136500; the National Nature Science Foundation of China under contract Nos 41890801 and 42076227; the Shanghai Pilot Program for Basic Research-Shanghai Jiao Tong University under contract No. 21TQ1400201.
*Corresponding author, E-mail: ruifengzhang@sjtu.edu.cn

elucidate their sources, sinks, and cycling in the marine environment. Isotopic ratios of these trace elements offer new insights into their biogeochemical cycles, sources, and sinks in the ocean (Sieber et al., 2019, 2021; Ellwood et al., 2020; Archer et al., 2020; Janssen et al., 2017; Lemaitre et al., 2020; Zhang et al., 2021; Little et al., 2018; Ruan et al., 2024) and reconstruct the paleoproductivity (Horner et al., 2021). For instance, in recent studies, anthropogenic aerosol iron fluxes have been traced in seawater (Conway et al., 2019; Pinedo-González et al., 2020). Furthermore, the domination of the sedimentary supply to the ocean interior by iron colloids (Homoky et al., 2021), strong fractionation of the Cd isotopes in seawater due to biological uptake (George et al., 2019), and the atmospheric inputs of isotopically light Cd on surface seawater (Sieber et al., 2023b) also have been reported. In recent Zn isotope studies, the controlling processes of Zn isotopes, including ligand binding and reversible scavenging (Sieber et al., 2023a) along with biological uptake of Zn (Vance et al., 2019) have been observed. The δ^{66}Zn variations on the ocean surface were particularly attributed to the phytoplankton uptake, anthropogenic Zn addition, and aerosol input in the Southern Ocean (Sieber et al., 2020), Atlantic Ocean (Lemaitre et al., 2020; Packman et al., 2022), and Northwest Pacific (Liao et al., 2020), respectively. The imbalances in the oceanic Ni budget have still not been fully resolved (Ciscato et al., 2018; Little et al., 2020). Recent studies have indicated that δ^{60}Ni is almost homogenous in the deep ocean (~1.3‰) and revealed a preferential uptake of isotopically light Ni by phytoplankton in surface waters (Archer et al., 2020; Yang et al., 2021; Lemaitre et al., 2022). The variations of δ^{65}Cu in surface water could be due to biological uptake (Baconnais et al., 2019), Cu ligand production, or new Cu sources, while only slight variations of δ^{65}Cu (0.6‰–0.7‰) have been reported in deep water (Little et al., 2018; Thompson and Ellwood, 2014; Takano et al., 2014).

Analyzing the isotopes of Fe, Ni, Cu, Zn, and Cd in seawater using samples of limited volumes presents several challenges. First, the concentrations of these metals in seawater are extremely low (Ni: 2–10 nmol/kg, Cu: 0.2–5 nmol/kg, Fe: 0.02–2 nmol/kg, Zn: 0.01–10 nmol/kg, and Cd: 1–1 000 pmol/kg) (de Baar et al., 1994; Moore and Braucher, 2007; Roshan et al., 2018; Richon and Tagliabue, 2019; John et al., 2022), increasing the potential for contamination and limiting the analytical precision (John and Adkins, 2010). Second, a high salt matrix content generates interferences and suppresses the signal voltages. Third, the unavailability of the double-spike technique for Cu requires a 100% yield to prevent isotopic fractionation (Hou et al., 2016).

Pretreatment and measurement methods for determining isotope ratios of Fe, Ni, Cu, Zn and Cd in seawater have been reported (Conway et al., 2013; Takano et al., 2017; Yang et al., 2020). The pretreatment procedure involved bulk extraction and purification steps. Bulk extraction in which the NOBIAS Chelate-PA1 resin is placed in a sample bottle to quantitatively capture transition metals, could concentrate metals in 1 L of seawater by up to 1 000 times (John and Adkins, 2010) with low procedural blanks. Isotope ratio measurements using multi-collector inductively coupled plasma mass spectroscopy (MC-ICPMS) employed the double-spike technique for Ni, Fe, Zn, and Cd and combined standard-sample bracketing with internal normalization method (C-SSBIN) for Cu. Besides correcting instrumental mass bias, the double-spike method can correct element fractionation caused by nonquantitative yields and accurately recalculate element concentrations through isotope dilution. The C-SSBIN method has improved the precision of isotopic ratios by at least two times comparing to the standard-sample bracketing method (Hou et al., 2016). However, there were only purification methods available for the simultaneous determination of, at most, three isotope systems (Conway et al., 2013; Takano et al., 2017). Conway et al. (2013) simultaneously separated Fe, Zn, and Cd using a single AG MP-1M resin microcolumn; However, Cu recovery was low and Ni elution occurred alongside the salt matrix with this chromatography. Yang et al. (2020) quantitatively separated Cu by employing a mixed solvent consisting of 11 mol/L acetic acid and 4 mol/L hydrochloric acid (HCl) to dissolve samples for loading columns and elute salts. This solvent markedly enhanced Cu recovery (Yang et al., 2019) compared to previous methods utilizing only HCl as the reagent (Maréchal et al., 1999; Takano et al., 2013; Hou et al., 2016; Paredes et al., 2018). Additionally, Yang et al. (2020) introduced a NOBIAS Chelate-PA1 resin column step to eliminate interfering elements from the Ni fraction. However, the purification column with a normal volume used above would elevate the blanks for Fe and Zn.

To address this, our novel method refined the existing methodologies, leading to the development of a streamlined and efficient technique for the isotopic analysis of Fe, Ni, Cu, Zn, and Cd in 1 L seawater. Additionally, we employed miniaturized polytetrafluoroethylene (PTFE) teflon microcolumns filled with 20 ng of AG MP-1M anion-exchange resin (Bio-Rad) to minimize the purification blanks. The developed technique involved a single chelating extraction process, followed by ion-exchange-based purifications, and isotopic analysis conducted using the Thermo Neptune MC-ICPMS.

2 Materials and method development

2.1 *Reagents, standards, and samples*

All samples were prepared using flow benches equipped with ultralow particulate air filters and located in the class-1000 clean laboratory of the School of Oceanography, Shanghai Jiao Tong University (SJTU). The reagents used in the study included Fisher Optima™ hydrobromic acid (HBr), hydrogen peroxide (H_2O_2), and ammonium hydroxide ($NH_3{\cdot}H_2O$). Fisher TraceMetal™ nitric acid (HNO_3), acetic acid (HAc) and Merck Suprapur® hydrochloric acid (HCl) were purified using a polyfluoroalkoxy (PFA) distillation system (Savillex® DST-1000) that employed sub-boiling distillation. Ultrapure water (>18.2 MΩ·cm, Milli-Q) obtained from a Q-POD element system (Merck) was used in the experiments. All acid-cleaned PFA teflon filtration apparatus and vials were sourced from Savillex. Acid-cleaned VWR metal-free 15 mL centrifuge tubes made of low-density polyethylene (LDPE) were used for eluent collection, isotopic analysis, and concentration analysis. The acid cleaning protocols used with all plastic labware were described in Zhang et al. (2015a). The Hitachi NOBIAS Chelate-PA1 resin and Bio-Rad AG MP-1M resin (100–200 mesh) were cleaned by soaking them three times over a week in 3 mol/L HNO_3 and 10% HCl, respectively, with extensive rinsing between the soakings. Before their use, the Hitachi NOBIAS Chelate-PA1 resin and Bio-Rad AG MP-1M resin were stored in 3 mol/L HNO_3 and ultrapure water, respectively.

A multielement standard (Inorganic™, IV-ICPMS-71A, 10 μg/mL 43 Element ICP Calibration/Quality Control Standard, including Al, Ba, Cd, Ce, Co, Dy, Eu, Ga, Fe, Pb, Mg, Nd, P, Pr, Sm, Ag, Sr, Tl, Tm, V, Zn, B, As, Be, Ca, Cr, Cu, Er, Gd, Ho, La, Lu, Mn, Ni, K, Rb, Se, Na, S, Th, U, Yb, Cs) was utilized to evaluate the pretreatment method, which included assessing the extraction efficiency, matrix element removal efficiency and purification yield.

Seawater samples obtained from the Chinese GEOTRACES subtropical Northwest Pacific (GP09) cruise and the Yellow Sea

cruise were employed for method development and validation. Samples of a full seawater column at Station K9 (11.00°N, 149.83°E) were collected by the R/V *Tan Kah Kee* during the GEOTRACES GP09 cruise (from April 25 to June 6, 2019) and the related data of Fe, Ni, Cu, Zn, and Cd concentrations have been reported by the study of Ge et al. (2022). Seawater samples were collected using the GEOTRACES trace element Carousel Sampling System equipped with 24 teflon-coated OTE Niskin-X bottles mounted on a trace-metal rosette system, deployed using a teflon-coated external spring (Ocean Test Equipment, USA). After its collection, seawater was filtered from the OTE Niskin-X bottles through Acropak capsules (0.2 μm) into precleaned 1 L LDPE bottles (Nalgene) in a class-1000 trace-metal clean van. All operations were performed according to the standard procedures recommended by the GEOTRACES program. The sample obtained during the Yellow Sea cruise (March/April 2022) was collected at 34.88°N, 121.68°E aboard the R/V *Xuelong*. It was obtained using X-Vane sampling assemblies (Zhang et al., 2015b) by mounting a 5 L Niskin-X bottle (comprising a teflon-coated inner bottle and teflon-coated external springs) at a depth of ~15 m upstream of a metal hydrowire with a weathering vane installed downstream of the bottle. The seawater sample was filtered through an Acropak capsule (0.2 μm) filter in a class 100 flow bench installed at the wet laboratory of the R/V *Xuelong*.

2.2 *Metal extraction from seawater*

The procedure used in sample handling and analysis is depicted in Tables 1 and 2. The seawater samples were acidified to a pH of ~2 at the clean laboratory of the SJTU by adding distilled HCl within 1–2 months after sample collection. The acidified samples were then stored for at least three months before performing the concentration and isotope analyses. The concentration of Cu was measured prior to the isotope analyses to determine the amounts of Zn internal standard to be added to each sample, and adjusted the Cu isotope standard concentration to match sample concentration using C-SSBIN method. The concentrations of Ni, Fe, Zn, and Cd were measured prior to the isotope analyses to determine the amounts of Ni, Fe, Zn, and Cd double spikes to be added to each sample using double-spike technique. Briefly, after pretreatment using a seaFAST automatic solid-phase extraction device, metal concentrations were quantified by the isotope dilution technique measured using a PerkinElmer PE-5000 triple quadrupole collision/reaction cell along with inductively coupled plasma mass spectrometry (ICP-

Table 1. Protocol for preconcentration of Ni, Cu, Fe, Zn and Cd by NOBIAS Chelate-PA1 resin

Step	Collection
a. Add ^{61}Ni–^{62}Ni, ^{57}Fe–^{58}Fe, ^{64}Zn–^{67}Zn, ^{110}Cd–^{111}Cd double spikes to 1 L seawater sample (pH = 2; 1 mmol/L H_2O_2) 72 h before extraction	–
b. Add 3 mL pre-cleaned resin in sample; shake for >5 h (Fe)	–
c. Adjust pH to 6.15 ± 0.2 with $CH_3CHOONH_4$ and $NH_3{\cdot}H_2O$; shake for >5 h (Ni, Cu, Zn, Cd)	–
d. Load sample through filter to separate resin	salts
e. Rinse resin with 125 mL ultrapure water	salts
f. Elute metals with (5 × 5) mL 3 mol/L HNO_3	metals
g. Evaporate samples at 200℃; redigest using 100 μL 16 mol/L HNO_3 and 100 μL 10 mol/L HCl to dissolve organics for >2 h	–
h. Evaporate samples at 200℃; redissolve in 200 μL 11 mol/L acetic acid + 4 mol/L HCl + 0.003% H_2O_2 for purification	–

Note: – represents no data.

Table 2. Protocol for purification of Ni, Cu, Fe, Zn and Cd for MC-ICPMS isotopic analysis

AG MP-1M purification step for Cu, Fe, Zn, Cd			
Step	Reagent	Volume/μL	Collection
Load AG MP-1M resin into PTFE microcolumns	Milli-Q water	20	–
Clean column	2 mol/L HNO_3	250 × 4	–
Rinse	ultrapure water	100 × 5	–
Condition	11 mol/L HAc + 4 mol/L HCl + 0.003% H_2O_2	100 × 2	–
Load sample	11 mol/L HAc + 4 mol/L HCl + 0.003% H_2O_2	200	Ni, Cr, V, salts
Elute Ni + salts	11 mol/L HAc + 4 mol/L HCl + 0.003% H_2O_2	20 × 7	Ni, Cr, V, salts
Elute Cu	5 mol/L HCl + 0.003% H_2O_2	20 × 20	Cu, Mn, Pb, Co
Elute Fe	1 mol/L HCl	20 × 9	Fe
Elute Zn	2 mol/L HNO_3 + 0.1 mol/L HBr	20 × 12	Zn
Elute Cd	2 mol/L HNO_3	20 × 10	Cd
NOBIAS Chelate-PA1-Ni purification step			
Step	Reagent	Volume/μL	Collection
Load NOBIAS Chelate-PA1 resin into PTFE microcolumns	Milli-Q water	20	–
Clean column	2 mol/L HNO_3	250 × 4	–
Rinse	ultrapure water	100 × 2	–
Condition	0.05 mol/L NH_4Ac (pH = 6)	100 × 2	–
Load sample	0.05 mol/L NH_4Ac (pH = 6)	200	salts, Cr
Elute salts	0.006 mol/L NH_4Ac (pH = 6)	20 × 7	salts
Elute Ni	2 mol/L HNO_3	20 × 7	Ni

Note: Reconstitution steps: (1) evaporate; (2) redigest using 200 μL 16 mol/L HNO_3 and 100 μL 30% H_2O_2 at 160℃ to dissolve organics for >6 h; (3) evaporate; (4) redissolve in 0.1 mol/L HNO_3 in 15 mL LDPE tubes for isotopic analysis. LDPE: low-density polyethylene; PTFE: polytetrafluoroethylene. – represents no data.

MS), as described by Ge et al. (2022).

Based on Conway et al. (2013), metals were extracted from seawater using a bulk extraction technique that employed the NOBIAS Chelate-PA1 cation-exchange resin. Along with lower blank results, the NOBIAS Chelate-PA1 resin demonstrates higher affinities to Zn and Cd compared with the IDA resin, and its affinity to Zn is also higher than that of the NTA resin (Conway et al., 2013). The concentration-matched double spikes containing ^{61}Ni–^{62}Ni, ^{57}Fe–^{58}Fe, ^{64}Zn–^{67}Zn, ^{110}Cd–^{111}Cd, and 100 μL of 30% H_2O_2 were added to 1 L of the acidified seawater samples and allowed to stand for at least 72 h. The samples were then treated with 3 mL of precleaned NOBIAS Chelate-PA1 resin and agitated for >5 h on a shaker table. To bring up the seawater pH to 6.15 ± 0.2, an ammonium acetate (NH_4Ac) buffer and $NH_3{\cdot}H_2O$ were added to the seawater, which was then continuously shaken for >5 h. The resin was subsequently passed through an acid-washed, 5-μm polycarbonate filter (Whatman), rinsed with ~125 mL of ultrapure water to eliminate salts, while metals were eluted with ~25 mL of 3 mol/L HNO_3 and collected in a 30-mL PFA beaker. The solution was then evaporated at 200℃ to dryness on a hot plate, digested using 100 μL 16 mol/L HNO_3 and 100 μL 10 mol/L HCl for at least 2 h, and evaporated to dryness once again. Finally, the samples were redissolved in 200 μL of 11 mol/L HAc + 4 mol/L HCl.

2.3 *Sample purification*

Following metal extraction, the samples underwent purification via microcolumn chromatography. The polytetrafluoroethylene (PTFE) teflon microcolumns were employed for minimizing the purification blanks (John and Adkins, 2010). These columns were fashioned using 5 mm inner diameter 4:1 heat-shrink PTFE tubing for a funnel shape. The final configuration of the column had a funnel tubing with a diameter of 1.25 mm and a height of approximately 20 mm, while the unheated funnel reservoir was about 10 mm in height. In this study, two anion-exchange purification methods from previously studies (Conway et al., 2013; Yang et al., 2020) were integrated to enable the concurrent purification of Ni, Cu, Fe, Zn, and Cd at low concentrations (0.2–200 ng/L). The full column purification protocols of the Ni, Cu, Fe, Zn, and Cd are provided in detail in Table 2. In brief, the samples were loaded onto 20 μL of precleaned and conditioned AG MP-1M resin in PTFE teflon microcolumns. Subsequently, the Ni + salts, Cu, Fe, Zn, and Cd were sequentially eluted using different reagents (AG MP-1M purification step; Table 2). The Ni fraction was then dried, redissolved in 200 μL of 0.05 mol/L NH_4Ac, and further purified on the NOBIAS Chelate-PA1 microcolumn to separate Ni from the matrix salts (NOBIAS Chelate-PA1-Ni step; Table 2). Following microcolumn chromatography, the final fractions of Ni, Cu, Fe, Zn, and Cd were dried in 7 mL PFA vials. The samples were then redigested using 200 μL of 16 mol/L HNO_3 and 100 μL of 30% H_2O_2 at 160℃ for about 6 h to decompose any residual organic matter, as described by Yang et al. (2019). The samples were dried again and redissolved in 0.1 mol/L HNO_3, then contained in 15-mL LDPE tubes for the isotopic analysis.

2.4 *Blanks and recovery efficiencies*

The procedural blanks for extraction were estimated by processing five replicates of 1 L of 0.01 mol/L HCl (pH = 2), only using the extraction procedure applied to the samples. The purification blanks were estimated from the five replicates by loading columns with 200 μL of 11 mol/L HAc + 4 mol/L HCl + 0.003% H_2O_2 for the AG MP-1M step and with 200 μL of 0.05 mol/L NH_4Ac for the NOBIAS Chelate-PA1-Ni step, followed by their purification processing as samples. The total procedural blanks were determined by processing five replicates of 1 L of 0.01 mol/L HCl (pH = 2) using the complete procedure applied to samples. The details will be discussed in Section 3.1.

The extraction efficiencies of the proposed method for Ni, Cu, Fe, Zn, and Cd were assessed by adding 200 μL of 1 μg/mL multielement standards (200 ng for all 43 elements) to ultrapure water, and extracting them as samples. The purification recoveries of the AG MP-1M step and NOBIAS Chelate-PA1-Ni step were determined by drying the multielement standards (200 ng for all 43 elements) and redissolving them in 200 μL of 11 mol/L HAc + 4 mol/L HCl, and 200 μL of 0.05 mol/L NH_4Ac respectively, and purifying them as samples. The original standard (untreated by either NOBIAS Chelate-PA1 or AG MP-1M) was used to calculate the recovery of the respective step. The recovered metal concentrations were determined using isotope dilution. We also obtained the total procedural recovery efficiencies from natural seawater samples by comparing the weights of samples before and after pretreatment. The metal weights of samples after the entire protocol were calculated based on the isotope dilution method, using isotope ratios from Neptune and the quantities of added spikes. The details will be discussed in Section 3.2.

2.5 *Isotopic measurement*

The Thermo Neptune Plus MC-ICPMS, equipped with a Ni Jet sample cone and an Al x-skimmer cone (Thermo Scientific), was employed for the analysis of δ^{56}Fe, δ^{60}Ni, δ^{65}Cu, δ^{66}Zn, and δ^{114}Cd, performed at the Southern Marine Science and Engineering Guangdong Laboratory (Zhuhai). In all isotope analyses performed, a PFA nebulizer with a flow rate of 100 μL/min and a quartz dual cyclonic spray chamber were employed for sample introduction. The isotopes of Cd and Cu were measured in the low-resolution mode (LR), while the isotopes of Fe, Zn, and Ni were measured in the high-resolution mode (HR) to circumvent potential polyatomic interferences (e.g., $^{40}Ar^{14}N^+$ on ^{54}Fe, $^{40}Ar^{16}O^+$ on ^{56}Fe, $^{40}Ar^{16}O^1H^+$ on ^{57}Fe, $^{40}Ar^{18}O^+$ on ^{58}Fe and ^{58}Ni, $^{40}Ar^{27}Al^+$ on ^{67}Zn, and $^{40}Ar^{28}Si^+$ on ^{68}Zn). These isotopes were resolved from their respective polyatomic interferences by measuring the signal voltages on the left flat shoulder of the combined metal-argide peak (Weyer and Schwieters, 2003). The proposed method achieved resolutions >7 000 ($m/\Delta m$; 5%–95% of the side of the peak) for Fe, Ni, and Zn. Typical representative sensitivities for ^{56}Fe (HR), ^{58}Ni (HR), ^{63}Cu (LR), ^{66}Zn (HR), and ^{114}Cd (LR) were 44 V, 32 V, 160 V, 15 V, and 110 V per ppm (10^{-6}), respectively.

To correct isobaric interferences, we measured their signal intensities for each isotope system, as indicated in the relevant cup configuration presented in Table 3. The ^{54}Cr and ^{58}Ni isobaric interferences on ^{54}Fe and ^{58}Fe were corrected by measuring the abundances of ^{53}Cr and ^{60}Ni, and the ^{58}Fe isobaric interference on ^{58}Ni was corrected by measuring the abundances of ^{57}Fe. Similarly, ^{64}Ni isobaric interference on ^{64}Zn was corrected by measuring the abundances of ^{60}Ni; ^{110}Pd, ^{112}Sn, and ^{114}Sn isobaric interferences on ^{110}Cd, ^{112}Cd, ^{114}Cd were corrected by measuring ^{105}Pd and ^{117}Sn (Table 3). Because Zn isotopes were used as the internal standard to correct for instrumental mass bias, ^{63}Cu, ^{65}Cu, ^{66}Zn and ^{64}Zn were measured simultaneously during Cu isotope analyses.

For δ^{56}Fe, δ^{60}Ni, δ^{66}Zn, and δ^{114}Cd, a double-spike technique was employed to correct for instrumental mass bias and any potential isotope fractionation during sample pretreatment. The data reduction scheme employed adhered to the algebraic approach described by Rudge et al. (2009). The Fe, Ni, Zn, and Cd double spikes primarily comprised 50% ^{57}Fe and 50% ^{58}Fe, 50%

Table 3. Cup configurations for Ni, Cu, Fe, Zn, Cd, and Fe isotopic analysis by Neptune MC-ICPMS

Faraday cup position	L4	L3	L2	L1	C	H1	H2	H3	H4
Ni (HR)	–	^{57}Fe	**^{58}Ni**	–	**^{60}Ni**	^{61}Ni	^{62}Ni	–	–
Cu (LR)	–	–	**^{63}Cu**	^{64}Zn	**^{65}Cu**	^{66}Zn	^{67}Zn	^{68}Zn	–
Fe (HR)	–	^{53}Cr	**^{54}Fe**	–	**^{56}Fe**	^{57}Fe	^{58}Fe	–	^{60}Ni
Zn (HR)	–	^{62}Ni	–	**^{64}Zn**	–	**^{66}Zn**	^{67}Zn	^{68}Zn	–
Cd (LR)	–	^{105}Pd	–	**^{110}Cd**	^{111}Cd	^{112}Cd	**^{114}Cd**	–	^{117}Sn

Note: Isotopes used in isotope ratios are bolded, while spiked isotopes are underlined. – represents no data.

^{61}Ni and 50% ^{62}Ni, 80% ^{64}Zn and 20% ^{67}Zn, and 33% ^{110}Cd and 66% ^{111}Cd, respectively to minimize errors occurring during data reduction (Rudge et al., 2009). A sample-spike ratio of 1:2 for Fe and 1:1 for Ni, Zn, and Cd were adopted to enhance analytical precision and reduce the potential impact of isobaric interference (John, 2012). Double spikes were prepared from monoisotopic solutions obtained from Isoflex USA, with concentrations determined by isotope dilution using the purchased concentration standards. Because Cu has only two stable isotopes, the double-spike technique cannot be used with Cu. Instead, C-SSBIN was used to correct for mass bias on the Cu isotope ratios (Takano et al., 2013, 2017). Zn isotope standard was added to the Cu isotope samples to serve as the internal standard, and the data reduction scheme followed was based on Hou et al. (2016) and Sullivan et al. (2020).

We used the solutions of the isotope standards IRMM-524a for Fe, NIST-986 for Ni, NIST-647 for Cu, NIST-3702 for Zn, and NIST-3108 for Cd. Isotope ratios of Fe, Cu, and Zn are traditionally expressed relative to IRMM-014, NIST-976, and Lyon JMC, respectively, which cannot be obtained now. IRMM-014 Fe δ^{56}Fe, NIST-976 Cu δ^{65}Cu, and Lyon JMC Zn δ^{66}Zn were −0.004‰ (2SD = 0.014‰), +0.2‰ (2SD = 0.02‰), and +0.28‰ (2SD = 0.02‰), respectively (Doucet et al., 2018; De Vega et al., 2020; Kidder et al., 2020) compared to IRMM-524a Fe, NIST-647 Cu, NIST-3702 Zn. Accordingly, corrections were applied to all data expressed relative to IRMM-014 Fe, NIST-976 Cu, and Lyon JMC Zn. In conclusion, we expressed Fe, Ni, Cu, Zn, and Cd isotope ratios using delta notation in per mil (‰) relative to the isotope standards IRMM-014 Fe, NIST-986 Ni, NIST-976 Cu, Lyon JMC Zn, and NIST-3108 Cd, as described in Eqs (1)–(5):

$$\delta^{56}\mathrm{Fe} = \left[\frac{\left(^{56}\mathrm{Fe}/^{54}\mathrm{Fe}\right)_{\mathrm{sample}}}{\left(^{56}\mathrm{Fe}/^{54}\mathrm{Fe}\right)_{\mathrm{IRMM\text{-}014}}} - 1\right] \times 1\,000‰, \quad (1)$$

$$\delta^{60}\mathrm{Ni} = \left[\frac{\left(^{60}\mathrm{Ni}/^{58}\mathrm{Ni}\right)_{\mathrm{sample}}}{\left(^{60}\mathrm{Ni}/^{58}\mathrm{Ni}\right)_{\mathrm{NIST\text{-}986}}} - 1\right] \times 1\,000‰, \quad (2)$$

$$\delta^{65}\mathrm{Cu} = \left[\frac{\left(^{65}\mathrm{Cu}/^{63}\mathrm{Cu}\right)_{\mathrm{sample}}}{\left(^{65}\mathrm{Cu}/^{63}\mathrm{Cu}\right)_{\mathrm{NIST\text{-}976}}} - 1\right] \times 1\,000‰, \quad (3)$$

$$\delta^{66}\mathrm{Zn} = \left[\frac{\left(^{66}\mathrm{Zn}/^{64}\mathrm{Zn}\right)_{\mathrm{sample}}}{\left(^{66}\mathrm{Zn}/^{64}\mathrm{Zn}\right)_{\mathrm{Lyon\text{-}JMC}}} - 1\right] \times 1\,000‰, \quad (4)$$

$$\delta^{114}\mathrm{Cd} = \left[\frac{\left(^{114}\mathrm{Cd}/^{110}\mathrm{Cd}\right)_{\mathrm{sample}}}{\left(^{114}\mathrm{Cd}/^{110}\mathrm{Cd}\right)_{\mathrm{NIST\text{-}3108}}} - 1\right] \times 1\,000‰. \quad (5)$$

The sequences required for the isotopic analysis using MC-ICPMS were conducted following the methodology outlined in Conway et al. (2013). At the commencement of each analytical session, the solutions of the isotope standards and pure double spikes were analyzed twice. Mixtures of the isotope standards and double spikes, matched for concentration, were used to bracket groups made of five samples. During the Cu isotopic measurement using the C-SSBIN approach, δ^{65}Cu values obtained by being bracketed by NIST-647 itself were utilized for monitoring instrumental stability, which exhibited an external precision of 0.02‰ (1SD, n = 83). Washout times were set as follows: rinsing in 0.5 mol/L HNO_3 for 2 min and in 0.1 mol/L HNO_3 for 1 min. Signal intensity was recorded over 50 cycles (each duration of 4.2 s), and the cycles exceeding three times the standard deviation were discarded. To correct for instrumental background, the average blank signal in a 0.1 mol/L HNO_3 solution was measured over 50 cycles. Each group of five samples was bracketed using two blank measurements.

3 Results and discussion

3.1 *Procedural blanks*

The procedural blanks for each step of the extraction and purification processes are listed in Table 4. The total procedural blanks of Ni, Cu, Fe, Zn, and Cd were (0.04 ± 0.05) ng, (0.04 ± 0.02) ng, (0.21 ± 0.20) ng, (0.15 ± 0.10) ng, and (3.0 ± 3.0) pg, respectively. The combined reagent blanks for sample extraction and subsequent purification, obtained by calculation, were less than the total blanks for each element, as revealed by the analysis of concentrated reagents that had been dried. Overall, our procedural blanks for Ni, Cu, Fe, Zn, and Cd were lower than those reported by John and Adkins (2010), Yang et al. (2020), and Takano et al. (2017) and were similar to those reported by Conway et al. (2013). These total procedural blanks are negligible when compared to the Ni, Cu, and Cd contents in 1 L of seawater

Table 4. The blanks (ng) in pretreatment steps of NOBIAS Chelate-PA1 resin extraction, AG MP-1M resin purification, NOBIAS Chelate-PA1 resin Ni purification, and total procedure (±1SD, n = 5)

Element	Extraction	AG MP-1M purification	NOBIAS Chelate-PA1-Ni purification	Total procedure	Reference comparison
Ni	0.04 ± 0.04	0.022 ± 0.000	0.004 ± 0.002	0.04 ± 0.05	⩽ 1[b]; 0.22[c]
Cu	0.05 ± 0.03	0.007 ± 0.001	–	0.04 ± 0.02	⩽ 1[b]; 0.29[c]
Fe	0.18 ± 0.10	0.069 ± 0.016	–	0.21 ± 0.20	1.1 ± 0.6[a]; 0.3[d]
Zn	0.16 ± 0.11	0.010 ± 0.002	–	0.15 ± 0.10	0.53[c]; 0.06[d]
Cd	0.001 ± 0.001	0.006 ± 0.003	–	0.003 ± 0.003	0.004[d]

Note: Total procedure blanks from recent studies are used for comparison. [a] John and Adkins (2010); [b] Yang et al. (2020); [c] Takano et al. (2017); [d] Conway et al. (2013). – represents no data.

obtained from the open ocean, which fall in the ranges of 100–600 ng Ni, 15–300 ng Cu, and 0.1–100 ng Cd. However, the total procedural blanks could potentially affect Fe and Zn, which have extremely low concentrations at the surface. In that case, a larger volume for preconcentration is recommended for Fe and Zn isotope measurements.

3.2 *Extraction efficiency and purification yield*

The extraction recoveries of Ni, Cu, Fe, Zn, and Cd are presented in Table 5, demonstrating the quantitative recovery of the elements. The quantitative recovery is required for Cu to avoid potential isotope fractionation during its extraction using the C-SSBIN method. The Fe, Zn, and Cd recoveries of bulk extraction from the study of Conway et al. (2013) were 78%, 101%, and 102%, respectively. Here we extended the shaking time for Fe from 2 h to 5 h to achieve an enhanced Fe extraction efficiency of 97.8% ± 1.4% (1SD, n = 5). We also could achieve a higher Cu recovery during bulk extraction than what was achieved by Yang et al. (2020), who reported a Cu extraction efficiency of 86% ± 2% (1SD) without adding any H_2O_2 prior to bulk extraction. This difference in the extraction efficiencies could be due to the addition of H_2O_2 to the samples (1 mmol/L H_2O_2 in each seawater sample), which destroyed the strong copper-binding ligands. The total procedural recovery efficiencies for Ni, Cu, Fe, Zn, and Cd were determined during the MC-ICPMS analysis of the seawater samples obtained from the Northwest Pacific and Yellow Sea. The total procedural recoveries for Ni, Cu, Fe, Zn, and Cd in the natural seawater samples were 98.3% ± 3.0%, 96.8% ± 1.6%, 92.8% ± 5.6%, 101.5% ± 3.8%, and 99.1% ± 3.3%, respectively. Besides, the seawater sample collected from the Yellow Sea was split into 14 samples and separately pretreated following procedure. Their extraction efficiencies for Ni, Cu, Fe, Zn, and Cd were 99.2% ± 2.1%, 99.8% ± 1.2%, 98.8% ± 1.6%, 100.2% ± 1.9%, and 99.5% ± 1.7%, respectively. These results showed comparable extraction efficiencies for seawater samples compared with ultrapure water supplemented with multielement standards.

Table 5. The recoveries in pretreatment steps of NOBIAS Chelate-PA1 resin extraction, AG MP-1M resin purification, and NOBIAS Chelate-PA1 resin Ni purification (±1SD, n = 5)

Element	Extraction	AG MP-1M purification	NOBIAS Chelate-PA1-Ni purification
Ni	100.5% ± 0.3%	99.8% ± 0.2%	99.7% ± 0.3%
Cu	100.2% ± 0.5%	99.5% ± 0.6%	–
Fe	97.8% ± 1.4%	99.1% ± 1.1%	–
Zn	99.9% ± 0.8%	99.5% ± 0.6%	–
Cd	100.1% ± 0.2%	99.7% ± 0.6%	–

Note: – represents no data.

Ni was purified using a two-step process (Table 2), with purification yields for each step listed in Table 4. Elution processes for interest metals (Fe, Ni, Cu, Zn, and Cd), as well as interfering elements in both the AG MP-1M step and the NOBIAS Chelate-PA1-Ni step, were examined alongside purification recovery testing using multielement standards, as shown in Fig. 1. In the AG MP-1M purification step, Cu, Fe, Zn, and Cd fractions were separated from interfering elements, while Ni was eluted alongside with salts (Fig. 1). The purification yields for Ni, Cu, Fe, Zn, and Cd in the AG MP-1M purification step were 99.8% ± 0.2%, 99.5% ± 0.6%, 99.1% ± 1.1%, 99.5% ± 0.6%, and 99.7% ± 0.6% (1SD, n = 5), respectively (Table 4). Figure 1 demonstrated the quantitative separation of salts from Cu, and salts, Cr, Ni from Fe, and salts, V, Cr, Ni from Zn, which avoided potential polyatomic interferences (e.g. $^{23}Na^{40}Ar^+$, $^{24}Mg^{40}Ar^+$, $^{44}Ca^{16}O^+$, $^{50}V^{16}O^+$, $^{51}V^{16}O^+$, $^{50}Cr^{16}O^+$, $^{52}Cr^{16}O^+$) (Gall et al., 2012; John and Adkins, 2010; Mason et al., 2004) and isobaric interferences (Fig. 5). Recent studies showed that Ti would be proportionally eluted into Cu and Ni fractions (Takano et al., 2017; Yang et al., 2020), resulting in polyatomic interferences (e.g. $^{47}Ti^{16}O^+$, $^{49}Ti^{14}N^+$, $^{49}Ti^{16}O^+$, $^{46}Ti^{16}O^+$). Also, Mn

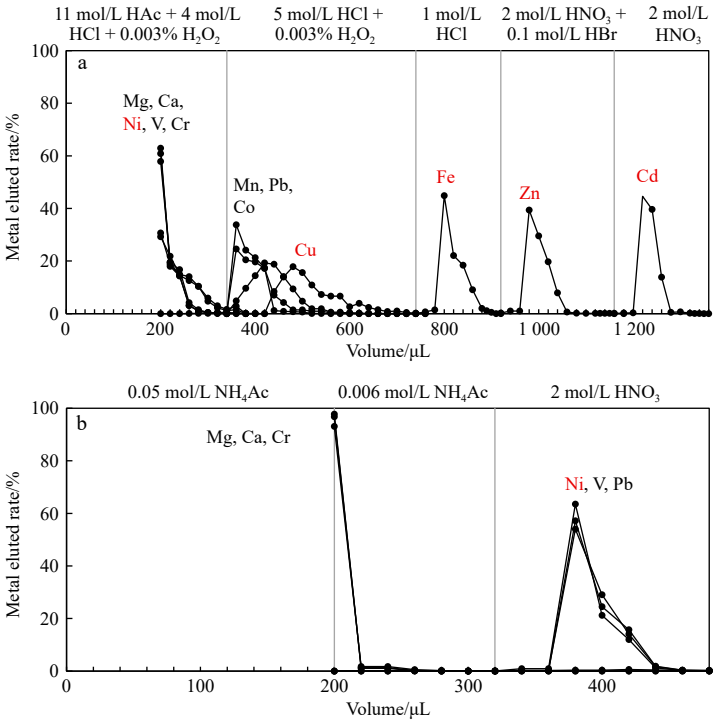

Fig. 1. Elution scheme for sample purification using an AG MP-1M resin microcolumn (a) and a NOBIAS Chelate-PA1 resin microcolumn (b). For the detailed protocols, see Table 2.

was eluted with Cu (Fig. 1), causing polyatomic interferences of $^{55}Mn^{14}N^+$, $^{55}Mn^{16}O^+$ on Ga (May and Wiedmeyer, 1998) when using Ga for mass bias correction measuring Cu isotopes. However, for our purification protocol, low concentration (0–300 pmol/L) of dissolved Ti in seawater samples (Orians et al., 1990) and using Zn for mass bias correction avoided further purification of Cu fraction after the AG MP-1M step, contrasting with purification protocols by Yang et al. (2020). Following the AG MP-1M purification step, Ni was effectively separated from the salts in the NOBIAS Chelate-PA1-Ni purification step (Fig. 1), which yielded 99.7% ± 0.3% (1SD, n = 5) recovery for Ni. Our results demonstrated the quantitative recovery of Ni, Cu, Fe, Zn, and Cd with low procedural blanks in purification steps.

3.3 *Analytical accuracy and isotopic analysis precision*

To evaluate the external error or accuracy of the proposed method, a series of isotope standards and double spikes were added to ultrapure water to simulate natural sample concentrations. The doped ultrapure water had to go through the entire process. The results obtained for δ^{56}Fe, δ^{60}Ni, δ^{65}Cu, δ^{66}Zn, and δ^{114}Cd were within the 1σ internal error obtained for all the concentrations by calculation (Fig. 2). Thus, the external errors could be considered negligible, and the internal error could be considered to represent the main error caused by Johnson noise and counting statistics (John, 2012; Conway et al., 2013).

Figure 3 presents the typical internal errors of Fe, Zn, Cd, and Ni isotope analyses using the double-spike method, which used seawater samples and natural isotope standard solutions. The measured internal errors (1σ) of Fe (n = 141), Ni (n = 56), Zn (n = 82), and Cd (n = 52) were fitted to the theoretical lines obtained from Monte Carlo simulation (John, 2012) using the double-spike toolbox (Rudge et al., 2009). Thus, we could use the fitted theoretical lines to estimate the internal error of a specific mass sample or the required sample volume. The fitted theoretical lines in Fig. 3 demonstrate that our proposed method can reliably determine δ^{56}Fe, δ^{60}Ni, δ^{66}Zn, and δ^{114}Cd in a 1 L seawater sample with concentrations as low as 0.2 nmol/kg (11 ng), 0.2 nmol/kg (12 ng), 0.4 nmol/kg (26 ng), and 0.1 nmol/kg (11 ng), respectively, with an accuracy <0.1‰ (1σ). Higher concentrations can yield higher accuracies for isotope analyses. However, in the surface ocean where Fe was 0.02 nmol/kg, the measured 1σ errors of a 2 L sample was 0.6‰. With regard to Cd in the surface ocean, which could be 0.01 nmol/kg, a 2 L sample was measured with 1σ errors of 0.5‰. The lowest surface concentration of Cd in the Northwest Pacific samples was 0.004 nmol/kg, which would result in an error (1σ) >1‰ for δ^{114}Cd using a 2 L sample, indicating that a large sample volume was required for a reliable δ^{114}Cd. The internal errors (1σ) of δ^{65}Cu obtained using 1 L of seawater sample were 0.02‰, 0.01‰, and 0.01‰ for Cu concentrations of 25 ng/kg, 50 ng/kg, and 100 ng/kg, respectively (Fig. 2), which are lower than the Cu concentrations in natural seawater samples. In summary, the 1σ internal errors for all five isotopes measured across the seawater profiles (δ^{56}Fe 0.02‰–0.6‰, δ^{60}Ni 0.01‰–0.03‰, δ^{65}Cu < 0.02‰, δ^{66}Zn 0.02‰–0.06‰, and δ^{114}Cd 0.03‰–1‰) were considerably smaller than the isotopic variability of each element in seawater (1‰–3‰) except for Cd and Fe in most of the surface ocean samples, which required larger sample volumes.

To examine the external precision of the proposed method when analyzing Fe, Ni, Cu, Zn, and Cd isotopes, the seawater

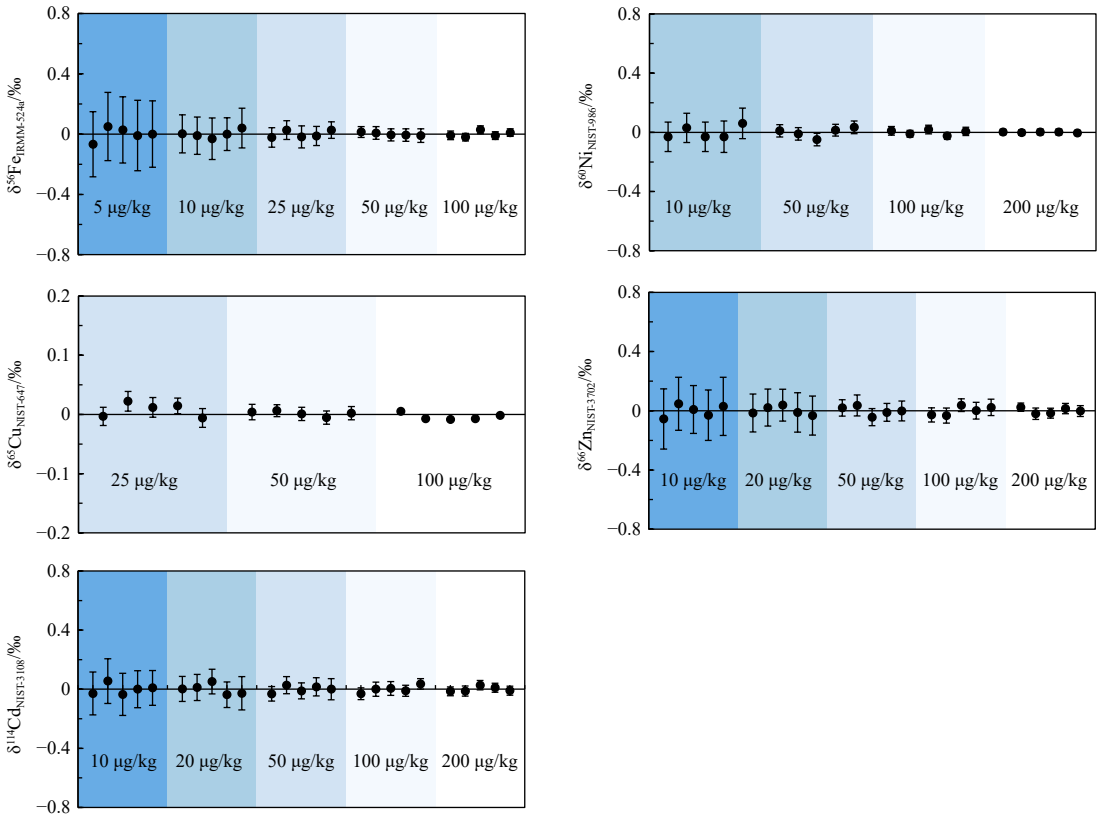

Fig. 2. δ^{56}Fe, δ^{60}Ni, δ^{65}Cu, δ^{66}Zn, and δ^{114}Cd values in ultrapure water doped with varying concentrations of natural isotope standards (IRMM-524a Fe, NIST-986 Ni, NIST-647 Cu, NIST-3702 Zn, and NIST-3108 Cd) measured according to the proposed method. Each concentration measurement included five replicates. Error bars represent the internal errors (1σ).

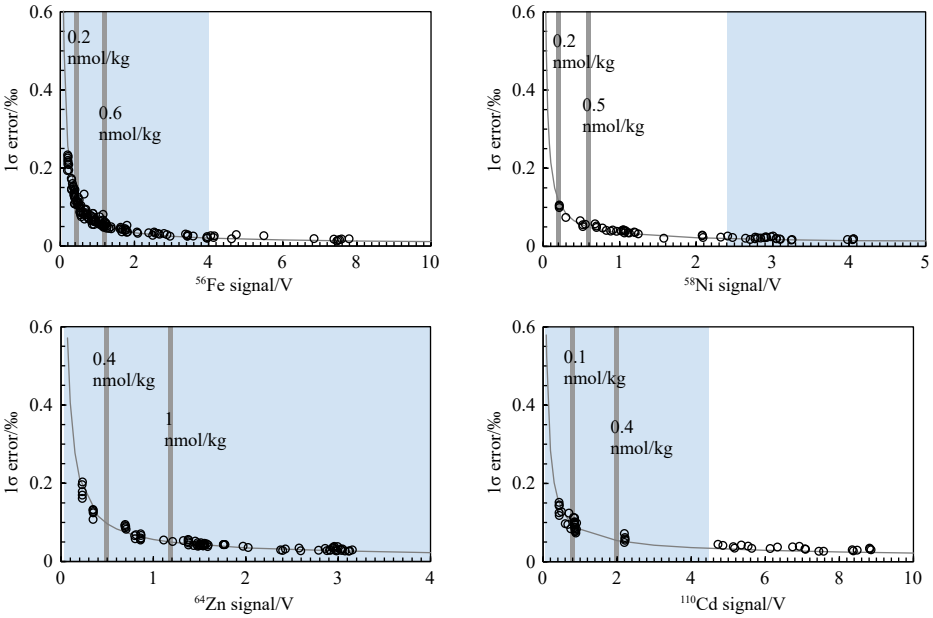

Fig. 3. Theoretical (gray line) versus measured (black points) 1σ internal errors of all samples for δ^{56}Fe, δ^{60}Ni, δ^{66}Zn, and δ^{114}Cd as compared to the MC-ICPMS signal. Theoretical lines were drawn based on Monte Carlo simulations. Vertical gray bars denote the seawater concentrations corresponding to 0.1‰ and 0.05‰ 1σ internal errors. Light blue rectangles indicate the range of signal intensities that correspond to 1 L nature seawater samples following their pretreatment based on the proposed method (de Baar et al., 1994; Moore and Braucher, 2007; Roshan et al., 2018; Richon and Tagliabue, 2019; John et al., 2022).

sample collected from the Yellow Sea (34.88°N, 121.68°E) was split into 14 samples and each of those samples was separately pretreated as set out in the proposed method. The average δ^{56}Fe, δ^{60}Ni, δ^{65}Cu, δ^{66}Zn, and δ^{114}Cd values with one standard deviation of the Yellow Sea seawater sample were –1.03‰ ± 0.03‰, 1.14‰ ± 0.03‰, 0.79‰ ± 0.02‰, 0.01‰ ± 0.03‰, and 0.63‰ ± 0.02‰, respectively, for element concentrations of (1.35 ± 0.02) nmol/kg, (7.75 ± 0.02) nmol/kg, (11.0 ± 0.02) nmol/kg, (1.98 ± 0.03) nmol/kg, and (0.32 ± 0.00) nmol/kg, respectively (Fig. 4). The results suggest that the external precisions of the method when analyzing Fe, Ni, Cu, Zn, and Cd isotopes are 0.03‰, 0.03‰, 0.02‰, 0.03‰, and 0.02‰, respectively, based on conservative estimations. The values obtained for the external precisions of the proposed method are comparable to the corresponding analytical internal errors.

3.4 *Method validation using GEOTRACES GP09-K9 profile samples*

To further validate the pretreatment method, we extracted and purified seawater samples obtained during the Chinese GEOTRACES GP09 cruise, and the results of dissolved δ^{56}Fe, δ^{60}Ni, δ^{66}Zn, and δ^{114}Cd isotopes and recalculated metal concentrations are presented in Fig. 5. The recalculated metal concentrations were determined based on the isotope dilution method, using isotope ratios from the Neptune and the quantities of added spikes. These recalculated metal concentrations showed good agreement with historical measurements by Ge et al. (2022), as their differences were less than 3%. Accordingly, these high-quality data are reasonable to be used for further elucidating the vertical distribution characteristics of Fe, Ni, Zn, and Cd in the subtropical Northwest Pacific. Furthermore, the concentrations of the trace metals in the Yellow Sea were consistent with those obtained in previous observations (Zhang et al., 2022).

Fe concentrations and isotopes from the K9 vertical profiles were similar to GR19 and GR21 profiles during the GP19 cruise which are available in the GEOTRACES Intermediate Data Product 2021 (https://www.bodc.ac.uk/geotraces/data/idp2021/). The heavy Fe isotopic composition in the chlorophyll maximum layer (at a depth of 80–180 m) indicated the influence of biological fractionation (König et al., 2021), while the light Fe isotope ratios at a depth of ~300 m characterized the contribution of North Pacific Intermediate Water (NPIW) (Conway and John, 2015a). The NPIW was indicated by salinity minimum (salinity < 34.5) lying around σ_θ = 26.7 (Fine et al., 1994). Positive Fe isotopes characteristic in deep water (750–5 000 m) revealed the deterministic role of dust supply on deep-ocean Fe of the Northwest Pacific, as the dissolved Fe released from dust always complexed with the organic ligand and showed a positive isotope signal (0.4‰–0.8‰) (Conway and John, 2014a; Fitzsimmons et al., 2015; John et al., 2018). The heavy δ^{56}Fe values of ~0.8‰ in the near-bottom (at a depth below 5 000 m) reflected a substantially nonreductive input of lithogenic Fe from the Lower Circumpolar Deep Water (LCDW) (Conway and John, 2014b; Abadie et al., 2017; John et al., 2018).

Ni concentrations and isotope ratios were comparable to their corresponding values in the GR03 Station (15°N, 165°E) in the Northwest Pacific (Takano et al., 2022). The increase in the δ^{60}Ni content from ~500 m toward the surface with a maximum value of 1.8‰ reflected the preferential phytoplankton uptake of light Ni isotopes in the surface water followed by the remineralization of biogenic particulates in deeper water (Takano et al., 2017; Archer et al., 2020; Yang et al., 2020, 2021). The Ni isotope composition in deeper water at depths below 500 m became nearly uniform, with mean values of 1.34‰ ± 0.02‰ (1SD, n = 12, Fig. 5), consistent with the deeper water δ^{60}Ni values observed in the global ocean (Takano et al., 2017, 2022; Wang et al., 2019; Archer et al., 2020; Yang et al., 2020, 2021).

The concentrations and isotope ratios distributions of Zn and Cd in Station K9 demonstrated strong agreement with the SAFe Station in the Northeast Pacific (30°N, 140°W) (Conway and John,

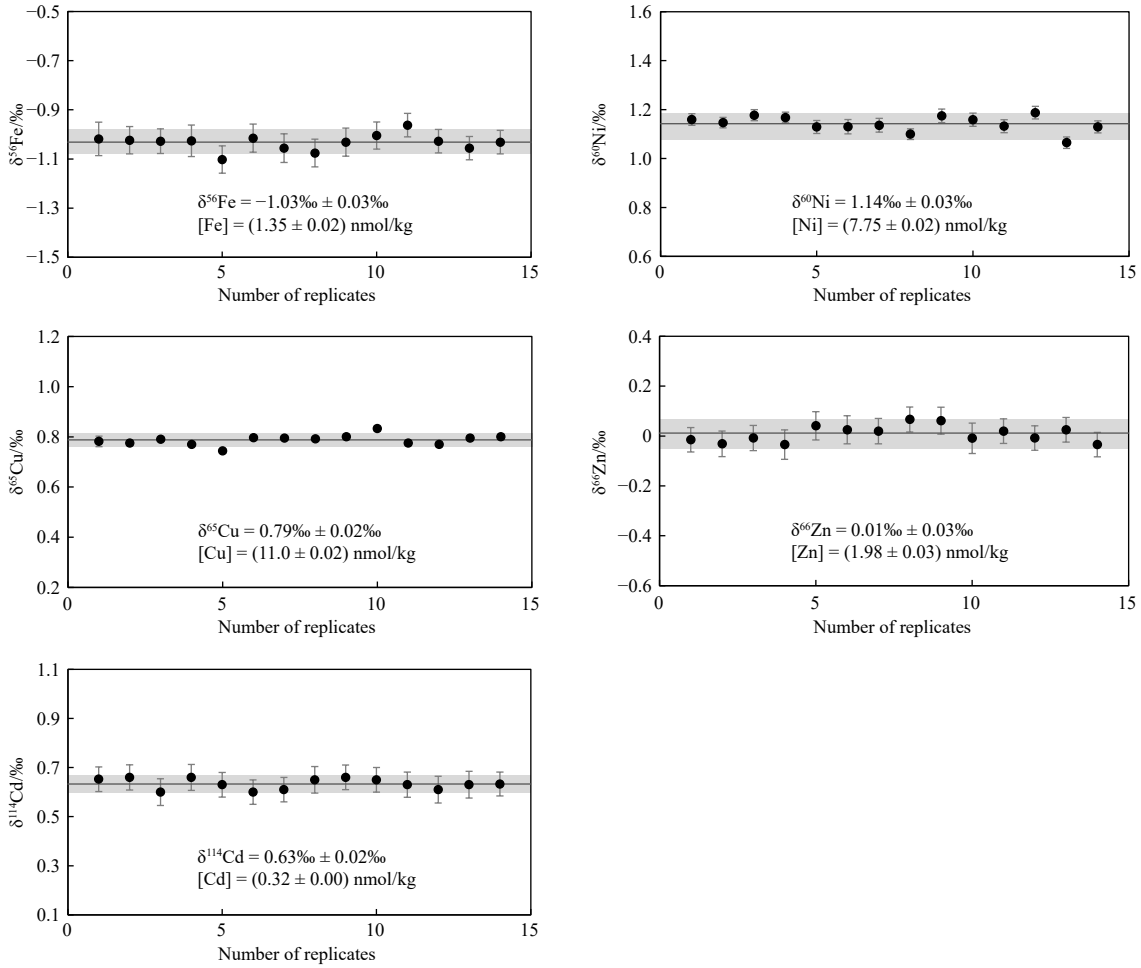

Fig. 4. External precisions for δ^{56}Fe, δ^{60}Ni, δ^{65}Cu, δ^{66}Zn, and δ^{114}Cd based on repeated pretreatment and analysis of a single seawater sample. The seawater sample was obtained at 34.88°N, 121.68°E from a depth of ~15 m during the Yellow Sea cruise (March/April 2022). Error bars represent the internal errors (1σ), while lines and gray bars depict the average isotope values and external precisions (average ± 1 SD), respectively.

2015a). Cd and Zn stable isotopes showed typical oceanic distribution characteristics and were influenced by both biological activities and large-scale water mass circulations (John and Conway, 2014; Abouchami et al., 2014; Zhang et al., 2019; Sieber et al., 2023a). The surface heavy Cd isotopes were caused by biological uptake within the euphotic zone (Conway and John, 2015b), while the surface light Zn isotopes resulted from the scavenging through the adsorption of isotopically heavy Zn to organic material (John and Conway, 2014; Coutaud et al., 2014). However, in deep waters, δ^{114}Cd (0.2‰–0.3‰) and δ^{66}Zn (~0.5‰) were fairly homogenous (Zhao et al., 2014; Conway and John, 2014b, 2015a; Sieber et al., 2023b).

4 Conclusions

In this study, we developed a new method for the simultaneous determination of five isotope systems (δ^{56}Fe, δ^{66}Zn, δ^{114}Cd, δ^{60}Ni, δ^{65}Cu) in a single 1 L seawater sample by incorporating and refining the methods previously proposed. The procedure involves only three pretreatment steps, including NOBIAS Chelate-PA1 resin extraction, AG MP-1M anion-exchange resin purification for Cu, Fe, Zn, and Cd, and NOBIAS Chelate-PA1 resin refinement to enable the separation of Ni from matrix elements. The separated elements were measured using the Thermo Neptune MC-ICPMS, employing the double-spike technique for Ni, Fe, Zn, Cd isotopes and the C-SSBIN method for Cu isotopes. The total procedural blanks for Ni, Cu, Fe, Zn, and Cd were 0.04 ng, 0.04 ng, 0.21 ng, 0.15 ng, and 3 pg, respectively, which are considered negligible in most seawater isotope analyses. High extraction efficiencies were achieved for Ni, Cu, Fe, Zn, and Cd at 100.5% ± 0.3%, 100.2% ± 0.5%, 97.8% ± 1.4%, 99.9% ± 0.8%, and 100.1% ± 0.2%, respectively. Quantitative recovery, low procedural blanks, coupled with double-spike and C-SSBIN techniques guaranteed the precision and accuracy of the method. The method accuracy was examined by analyzing Milli-Q water doped with various concentrations of isotope standards, demonstrating isotope values within the 1σ internal error for all the concentrations. Repeated analyses using 1 L of Yellow Sea seawater samples indicated an external precision of 0.03‰, 0.02‰, 0.03‰, 0.04‰, and 0.03‰ (1SD; n = 14) for δ^{60}Ni, δ^{65}Cu, δ^{56}Fe, δ^{66}Zn, and δ^{114}Cd, respectively. Additionally, the proposed method was validated using the seawater samples of the Station K9 vertical profiles obtained during a Chinese GEOTRACES GP09 cruise in the Northwest Pacific. The profiles of δ^{56}Fe, δ^{66}Zn, δ^{114}Cd, and δ^{60}Ni demonstrated good agreement with previous related data or studies. Furthermore, we reported the δ^{56}Fe vertical profiles in the Northwest Pacific for the first time, revealing influences for Fe from biological fractionation (80–180 m), NPIW (200–500 m), Fe resulting from dust deposition chelated by or-

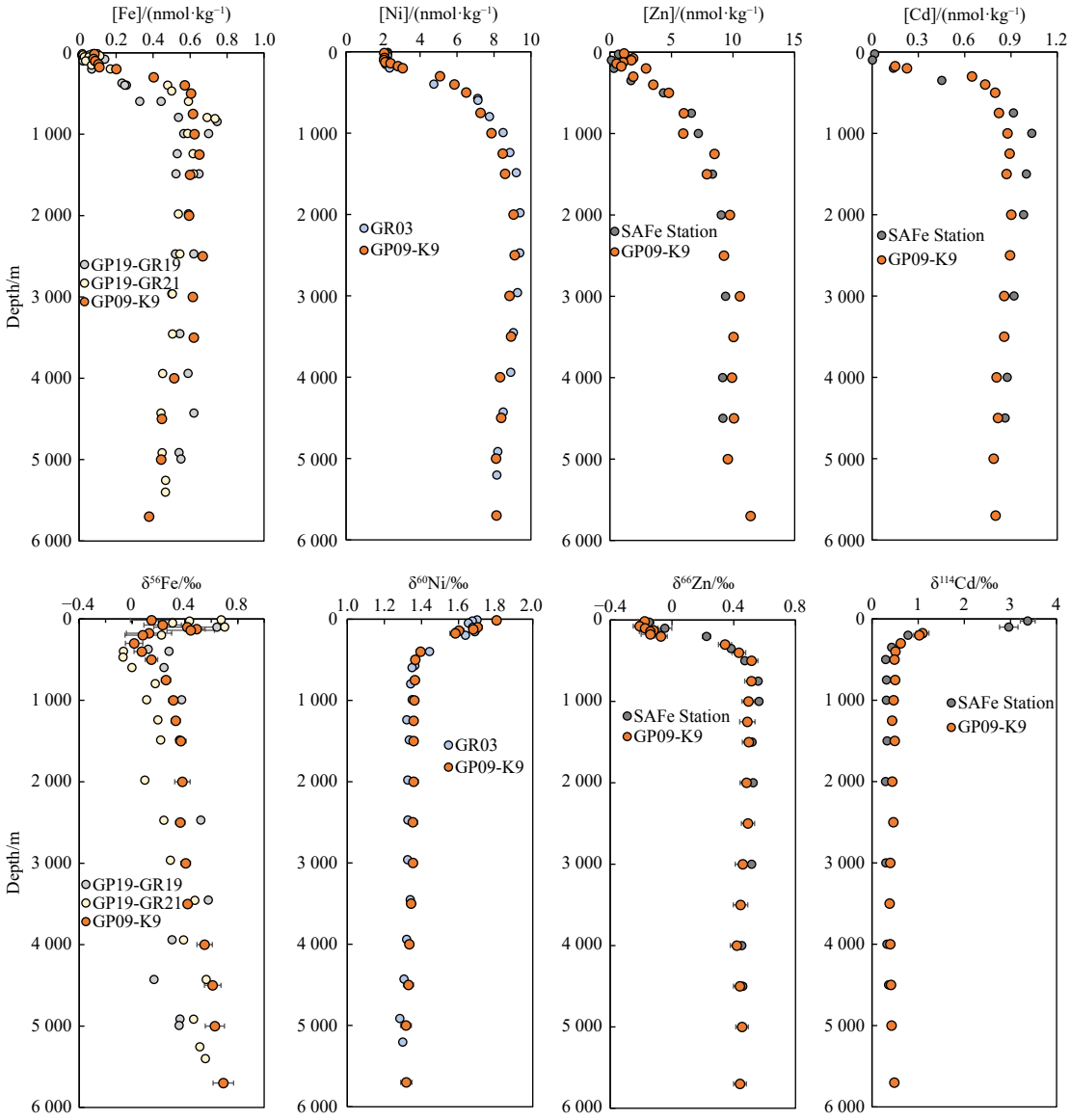

Fig. 5. Concentrations and stable isotope profiles of the samples collected at Station K9 (11°N, 150°E) along the GEOTRACES cruise GP09 in the Northwest Pacific compared with the GR19 and GR21 profiles obtained from the GEOTRACES Intermediate Data Product 2021 during the GP19 cruise (https://www.bodc.ac.uk/geotraces/data/idp2021/), SAFe Station (30°N, 140°W) in the Northeast Pacific (Conway and John, 2015a), and GR03 Station (15°N, 165°E) in the Northwest Pacific (Takano et al., 2022). Error bars represent the 1σ internal errors of the isotopic analysis.

ganic ligand (750–5 000 m), and LCDW (>5 000 m) from the surface ocean to the deep ocean. The stable isotopes of Ni, Zn, and Cd were consistent with typical oceanic distributions, influenced by biological activity, reversible scavenging, and large-scale water mass circulations. We believe that the proposed method will encourage researchers to handle the chromatography of systems with a large number of isotopes, enhancing our understanding of the oceanic biogeochemical cycles of Ni, Cu, Fe, Zn, and Cd.

Acknowledgements

We would like to thank the Southern Marine Science and Engineering Guangdong Laboratory (Zhuhai) for the instrumental support for isotopic determination. This work was also supported by the Shanghai Frontiers Science Center of Polar Science.

References

Abadie C, Lacan F, Radic A, et al. 2017. Iron isotopes reveal distinct dissolved iron sources and pathways in the intermediate versus deep Southern Ocean. Proceedings of the National Academy of Sciences of the United States of America, 114(5): 858–863, doi: 10.1073/pnas.1603107114

Abouchami W, Galer S J G, De Baar H J W, et al. 2014. Biogeochemical cycling of cadmium isotopes in the Southern Ocean along the Zero Meridian. Geochimica et Cosmochimica Acta, 127: 348–367, doi: 10.1016/j.gca.2013.10.022

Alfano M, Cavazza C. 2020. Structure, function, and biosynthesis of nickel-dependent enzymes. Protein Science, 29(5): 1071–1089, doi: 10.1002/pro.3836

Archer C, Vance D, Milne A, et al. 2020. The oceanic biogeochemistry of nickel and its isotopes: new data from the South Atlantic and the Southern Ocean biogeochemical divide. Earth and Planetary Science Letters, 535: 116118, doi: 10.1016/j.epsl.2020.116118

Baconnais I, Rouxel O, Dulaquais G, et al. 2019. Determination of the copper isotope composition of seawater revisited: a case study from the Mediterranean Sea. Chemical Geology, 511: 465–480,

doi: 10.1016/j.chemgeo.2018.09.009
Boyd P W, Ellwood M J. 2010. The biogeochemical cycle of iron in the ocean. Nature Geoscience, 3(10): 675–682, doi: 10.1038/ngeo964
Ciscato E R, Bontognali T R R, Vance D. 2018. Nickel and its isotopes in organic-rich sediments: implications for oceanic budgets and a potential record of ancient seawater. Earth and Planetary Science Letters, 494: 239–250, doi: 10.1016/j.epsl.2018.04.061
Conway T M, Hamilton D S, Shelley R U, et al. 2019. Tracing and constraining anthropogenic aerosol iron fluxes to the North Atlantic Ocean using iron isotopes. Nature Communications, 10(1): 2628, doi: 10.1038/s41467-019-10457-w
Conway T M, John S G. 2015a. The cycling of iron, zinc and cadmium in the North East Pacific Ocean–insights from stable isotopes. Geochimica et Cosmochimica Acta, 164: 262–283, doi: 10.1016/j.gca.2015.05.023
Conway T M, John S G. 2015b. Biogeochemical cycling of cadmium isotopes along a high-resolution section through the North Atlantic Ocean. Geochimica et Cosmochimica Acta, 148: 269–283, doi: 10.1016/j.gca.2014.09.032
Conway T M, John S G. 2014a. Quantification of dissolved iron sources to the North Atlantic Ocean. Nature, 511(7508): 212–215, doi: 10.1038/nature13482
Conway T M, John S G. 2014b. The biogeochemical cycling of zinc and zinc isotopes in the North Atlantic Ocean. Global Biogeochemical Cycles, 28(10): 1111–1128, doi: 10.1002/2014GB004862
Conway T M, Rosenberg A D, Adkins J F, et al. 2013. A new method for precise determination of iron, zinc and cadmium stable isotope ratios in seawater by double-spike mass spectrometry. Analytica Chimica Acta, 793: 44–52, doi: 10.1016/j.aca.2013.07.025
Coutaud A, Meheut M, Viers J, et al. 2014. Zn isotope fractionation during interaction with phototrophic biofilm. Chemical Geology, 390: 46–60, doi: 10.1016/j.chemgeo.2014.10.004
de Baar H J W, Saager P M, Nolting R F, et al. 1994. Cadmium versus phosphate in the world ocean. Marine Chemistry, 46(3): 261–281, doi: 10.1016/0304-4203(94)90082-5
Doucet L S, Laurent O, Mattielli N, et al. 2018. Zn isotope heterogeneity in the continental lithosphere: new evidence from Archean granitoids of the northern Kaapvaal craton, South Africa. Chemical Geology, 476: 260–271, doi: 10.1016/j.chemgeo.2017.11.022
Ellwood M J, Strzepek R F, Strutton P G, et al. 2020. Distinct iron cycling in a Southern Ocean eddy. Nature Communications, 11(1): 825, doi: 10.1038/s41467-020-14464-0
Falkowski P G, Barber R T, Smetacek V. 1998. Biogeochemical controls and feedbacks on ocean primary production. Science, 281(5374): 200–206, doi: 10.1126/science.281.5374.200
Fine R A, Lukas R, Bingham F M, et al. 1994. The western equatorial Pacific: a water mass crossroads. Journal of Geophysical Research: Oceans, 99(C12): 25063–25080, doi: 10.1029/94JC02277
Fitzsimmons J N, Carrasco G G, Wu Jingfeng, et al. 2015. Partitioning of dissolved iron and iron isotopes into soluble and colloidal phases along the GA03 GEOTRACES North Atlantic Transect. Deep-Sea Research Part II: Topical Studies in Oceanography, 116: 130–151, doi: 10.1016/j.dsr2.2014.11.014
Gall L, Williams H, Siebert C, et al. 2012. Determination of mass-dependent variations in nickel isotope compositions using double spiking and MC-ICPMS. Journal of Analytical Atomic Spectrometry, 27(1): 137–145, doi: 10.1039/C1JA10209E
Ge Yuncong, Zhang Ruifeng, Jiang Ziyuan, et al. 2022. Determination of Fe, Ni, Cu, Zn, Cd and Pb in seawater by isotope dilution automatic solid-phase extraction—ICP-MS. Acta Oceanologica Sinica, 41(8): 129–136, doi: 10.1007/s13131-022-2016-2
George E, Stirling C H, Gault-Ringold M, et al. 2019. Marine biogeochemical cycling of cadmium and cadmium isotopes in the extreme nutrient-depleted subtropical gyre of the South West Pacific Ocean. Earth and Planetary Science Letters, 514: 84–95, doi: 10.1016/j.epsl.2019.02.031
de Vega C G, Chernonozhkin S M, Grigoryan R, et al. 2020. Characterization of the new isotopic reference materials IRMM-524A and ERM-AE143 for Fe and Mg isotopic analysis of geological and biological samples. Journal of Analytical Atomic Spectrometry, 35(11): 2517–2529, doi: 10.1039/D0JA00225A
Homoky W B, Conway T M, John S G, et al. 2021. Iron colloids dominate sedimentary supply to the ocean interior. Proceedings of the National Academy of Sciences of the United States of America, 118(13): e2016078118, doi: 10.1073/pnas.2016078118
Horner T J, Little S H, Conway T M, et al. 2021. Bioactive trace metals and their isotopes as paleoproductivity proxies: an assessment using GEOTRACES-era data. Global Biogeochemical Cycles, 35(11): e2020GB006814, doi: 10.1029/2020GB006814
Hou Qinghua, Zhou Lian, Gao Shan, et al. 2016. Use of Ga for mass bias correction for the accurate determination of copper isotope ratio in the NIST SRM 3114 Cu standard and geological samples by MC-ICPMS. Journal of Analytical Atomic Spectrometry, 31(1): 280–287, doi: 10.1039/C4JA00488D
Janssen D J, Abouchami W, Galer S J G, et al. 2017. Fine-scale spatial and interannual cadmium isotope variability in the subarctic Northeast Pacific. Earth and Planetary Science Letters, 472: 241–252, doi: 10.1016/j.epsl.2017.04.048
John S G. 2012. Optimizing sample and spike concentrations for isotopic analysis by double-spike ICPMS. Journal of Analytical Atomic Spectrometry, 27(12): 2123–2131, doi: 10.1039/C2JA30215B
John S G, Adkins J F. 2010. Analysis of dissolved iron isotopes in seawater. Marine Chemistry, 119(1–4): 65–76, doi: 10.1016/j.marchem.2010.01.001
John S G, Conway T M. 2014. A role for scavenging in the marine biogeochemical cycling of zinc and zinc isotopes. Earth and Planetary Science Letters, 394: 159–167, doi: 10.1016/j.epsl.2014.02.053
John S G, Helgoe J, Townsend E, et al. 2018. Biogeochemical cycling of Fe and Fe stable isotopes in the eastern Tropical South Pacific. Marine Chemistry, 201: 66–76, doi: 10.1016/j.marchem.2017.06.003
John S G, Kelly R L, Bian Xiaopeng, et al. 2022. The biogeochemical balance of oceanic nickel cycling. Nature Geoscience, 15(11): 906–912, doi: 10.1038/s41561-022-01045-7
Kidder J A, Voinot A, Sullivan K V, et al. 2020. Improved ion-exchange column chromatography for Cu purification from high-Na matrices and isotopic analysis by MC-ICPMS. Journal of Analytical Atomic Spectrometry, 35(4): 776–783, doi: 10.1039/C9JA00359B
König D, Conway T M, Ellwood M J, et al. 2021. Constraints on the cycling of iron isotopes from a global ocean model. Global Biogeochemical Cycles, 35(9): e2021GB006968, doi: 10.1029/2021GB006968
Lane T W, Morel F M M. 2000. A biological function for cadmium in marine diatoms. Proceedings of the National Academy of Sciences of the United States of America, 97(9): 4627–4631, doi: 10.1073/pnas.090091397
Lemaitre N, de Souza G F, Archer C, et al. 2020. Pervasive sources of isotopically light zinc in the North Atlantic Ocean. Earth and Planetary Science Letters, 539: 116216, doi: 10.1016/j.epsl.2020.116216
Lemaitre N, Du Jianghui, de Souza G F, et al. 2022. The essential bioactive role of nickel in the oceans: evidence from nickel isotopes. Earth and Planetary Science Letters, 584: 117513, doi: 10.1016/j.epsl.2022.117513
Liao Wen-Hsuan, Takano S, Yang Shun-Chung, et al. 2020. Zn isotope composition in the water column of the northwestern Pacific Ocean: the importance of external sources. Global Biogeochemical Cycles, 34(1): e2019GB006379, doi: 10.1029/2019GB006379
Little S H, Archer C, McManus J, et al. 2020. Towards balancing the oceanic Ni budget. Earth and Planetary Science Letters, 547: 116461, doi: 10.1016/j.epsl.2020.116461
Little S H, Archer C, Milne A, et al. 2018. Paired dissolved and particulate phase Cu isotope distributions in the South Atlantic. Chemical Geology, 502: 29–43, doi: 10.1016/j.chemgeo.2018.07.

022
Maréchal C N, Télouk P, Albarède F. 1999. Precise analysis of copper and zinc isotopic compositions by plasma-source mass spectrometry. Chemical Geology, 156(1–4): 251–273, doi: 10.1016/S0009-2541(98)00191-0
Mason T F D, Weiss D J, Horstwood M, et al. 2004. High-precision Cu and Zn isotope analysis by plasma source mass spectrometry part 1. Spectral interferences and their correction. Journal of Analytical Atomic Spectrometry, 19(2): 209–217, doi: 10.1039/B306958C
SCOR Working Group. 2007. GEOTRACES-an international study of the global marine biogeochemical cycles of trace elements and their isotopes. Geochemistry, 67(2): 85–131, doi: 10.1016/j.chemer.2007.02.001
Middag R, van Heuven S M A C, Bruland K W, et al. 2018. The relationship between cadmium and phosphate in the Atlantic Ocean unravelled. Earth and Planetary Science Letters, 492: 79–88, doi: 10.1016/j.epsl.2018.03.046
May T W, Wiedmeyer R H. 1998. A table of polyatomic interferences in ICP-MS. Atomic Spectroscopy, 19(5): 150–155
Moore J K, Braucher O. 2007. Observations of dissolved iron concentrations in the World Ocean: implications and constraints for ocean biogeochemical models. Biogeosciences Discuss, 4(2): 1241–1277
Morel F M M, Price N M. 2003. The biogeochemical cycles of trace metals in the oceans. Science, 300(5621): 944–947, doi: 10.1126/science.1083545
Orians K J, Boyle E A, Bruland K W. 1990. Dissolved titanium in the open ocean. Nature, 348(6299): 322–325, doi: 10.1038/348322a0
Packman H, Little S H, Baker A R, et al. 2022. Tracing natural and anthropogenic sources of aerosols to the Atlantic Ocean using Zn and Cu isotopes. Chemical Geology, 610: 1–14, doi: 10.1016/j.chemgeo.2022.121091
Paredes E, Avazeri E, Malard V, et al. 2018. A new procedure for high precision isotope ratio determinations of U, Cu and Zn at nanogram levels in cultured human cells: what are the limiting factors?. Talanta, 178: 894–904, doi: 10.1016/j.talanta.2017.10.046
Payne C D, Price N M. 1999. Effects of cadmium toxicity on growth and elemental composition of marine phytoplankton. Journal of Phycology, 35(2): 293–302, doi: 10.1046/j.1529-8817.1999.3520293.x
Pinedo-González P, Hawco N J, Bundy R M, et al. 2020. Anthropogenic Asian aerosols provide Fe to the North Pacific Ocean. Proceedings of the National Academy of Sciences of the United States of America, 117(45): 27862–27868, doi: 10.1073/pnas.2010315117
Price N M, Morel F M M. 1990. Cadmium and cobalt substitution for zinc in a marine diatom. Nature, 344(6267): 658–660, doi: 10.1038/344658a0
Richon C, Tagliabue A. 2019. Insights into the major processes driving the global distribution of copper in the ocean from a global model. Global Biogeochemical Cycles, 33(12): 1594–1610, doi: 10.1029/2019GB006280
Roshan S, DeVries T, Wu Jingfeng, et al. 2018. The internal cycling of zinc in the ocean. Global Biogeochemical Cycles, 32(12): 1833–1849, doi: 10.1029/2018GB006045
Ruan Yaqing, Zhang Ruifeng, Yang Shun-Chung, et al. 2024. Iron, Nickel, Copper, Zinc, and their stable isotopes along a salinity gradient in the Pearl River Estuary, southeastern China. Chemical Geology, 645: 121893, doi: 10.1016/j.chemgeo.2023.121893
Rudge J F, Reynolds B C, Bourdon B. 2009. The double spike toolbox. Chemical Geology, 265(3–4): 420–431, doi: 10.1016/j.chemgeo.2009.05.010
Sieber M, Conway T M, de Souza G F, et al. 2021. Isotopic fingerprinting of biogeochemical processes and iron sources in the iron-limited surface Southern Ocean. Earth and Planetary Science Letters, 567: 116967, doi: 10.1016/j.epsl.2021.116967
Sieber M, Conway T M, de Souza G F, et al. 2020. Cycling of zinc and its isotopes across multiple zones of the Southern Ocean: insights from the Antarctic Circumnavigation Expedition. Geochimica et Cosmochimica Acta, 268: 310–324, doi: 10.1016/j.gca.2019.09.039
Sieber M, Conway T M, de Souza G F, et al. 2019. High-resolution Cd isotope systematics in multiple zones of the Southern Ocean from the Antarctic Circumnavigation Expedition. Earth and Planetary Science Letters, 527: 115799, doi: 10.1016/j.epsl.2019.115799
Sieber M, Lanning N T, Bian Xiaopeng, et al. 2023a. The importance of reversible scavenging for the marine Zn cycle evidenced by the distribution of zinc and its isotopes in the Pacific Ocean. Journal of Geophysical Research: Oceans, 128(4): e2022JC019419, doi: 10.1029/2022JC019419
Sieber M, Lanning N T, Bunnell Z B, et al. 2023b. Biological, physical, and atmospheric controls on the distribution of cadmium and its isotopes in the Pacific Ocean. Global Biogeochemical Cycles, 37(2): e2022GB007441, doi: 10.1029/2022GB007441
Sullivan K, Layton-Matthews D, Leybourne M, et al. 2020. Copper isotopic analysis in geological and biological reference materials by MC-ICP-MS. Geostandards and Geoanalytical Research, 44(2): 349–362, doi: 10.1111/ggr.12315
Tagliabue A, Bowie A R, Boyd P W, et al. 2017. The integral role of iron in ocean biogeochemistry. Nature, 543(7643): 51–59, doi: 10.1038/nature21058
Takano S, Liao Wen-Hsuan, Ho Tung-Yuan, et al. 2022. Isotopic evolution of dissolved Ni, Cu, and Zn along the Kuroshio through the East China Sea. Marine Chemistry, 243: 104135, doi: 10.1016/j.marchem.2022.104135
Takano S, Tanimizu M, Hirata T, et al. 2017. A simple and rapid method for isotopic analysis of nickel, copper, and zinc in seawater using chelating extraction and anion exchange. Analytica Chimica Acta, 967: 1–11, doi: 10.1016/j.aca.2017.03.010
Takano S, Tanimizu M, Hirata T, et al. 2014. Isotopic constraints on biogeochemical cycling of copper in the ocean. Nature Communications, 5: 5663, doi: 10.1038/ncomms6663
Takano S, Tanimizu M, Hirata T, et al. 2013. Determination of isotopic composition of dissolved copper in seawater by multi-collector inductively coupled plasma mass spectrometry after preconcentration using an ethylenediaminetriacetic acid chelating resin. Analytica Chimica Acta, 784: 33–41, doi: 10.1016/j.aca.2013.04.032
Thompson C M, Ellwood M J. 2014. Dissolved copper isotope biogeochemistry in the Tasman Sea, SW Pacific Ocean. Marine Chemistry, 165: 1–9, doi: 10.1016/j.marchem.2014.06.009
Twining B S, Baines S B. 2013. The trace metal composition of marine phytoplankton. Annual Review of Marine Science, 5: 191–215, doi: 10.1146/annurev-marine-121211-172322
Vance D, de Souza G F, Zhao Ye, et al. 2019. The relationship between zinc, its isotopes, and the major nutrients in the North-East Pacific. Earth and Planetary Science Letters, 525: 115748, doi: 10.1016/j.epsl.2019.115748
Wang Ruomei, Archer C, Bowie A R, et al. 2019. Zinc and nickel isotopes in seawater from the Indian Sector of the Southern Ocean: the impact of natural iron fertilization versus Southern Ocean hydrography and biogeochemistry. Chemical Geology, 511: 452–464, doi: 10.1016/j.chemgeo.2018.09.010
Weber T, John S, Tagliabue A, et al. 2018. Biological uptake and reversible scavenging of zinc in the global ocean. Science, 361(6397): 72–76, doi: 10.1126/science.aap8532
Weyer S, Schwieters J B. 2003. High precision Fe isotope measurements with high mass resolution MC-ICPMS. International Journal of Mass Spectrometry, 226(3): 355–368, doi: 10.1016/S1387-3806(03)00078-2
Yang Shun-Chung, Hawco N J, Pinedo-González P, et al. 2020. A new purification method for Ni and Cu stable isotopes in seawater provides evidence for widespread Ni isotope fractionation by phytoplankton in the North Pacific. Chemical Geology, 547: 119662, doi: 10.1016/j.chemgeo.2020.119662
Yang Shun-Chung, Kelly R L, Bian Xiaopeng, et al. 2021. Lack of redox cycling for nickel in the water column of the eastern Tropical North Pacific oxygen deficient zone: insight from dissolved and particulate nickel isotopes. Geochimica et

Cosmochimica Acta, 309: 235–250, doi: 10.1016/j.gca.2021.07.004

Yang Shun-Chung, Welter L, Kolatkar A, et al. 2019. A new anion exchange purification method for Cu stable isotopes in blood samples. Analytical and Bioanalytical Chemistry, 411(3): 765–776, doi: 10.1007/s00216-018-1498-4

Zhang Ruifeng, Jensen L, Fitzsimmons J, et al. 2021. Iron isotope biogeochemical cycling in the western Arctic Ocean. Global Biogeochemical Cycles, 35(11): e2021GB006977, doi: 10.1029/2021GB006977

Zhang Ruifeng, Jensen L T, Fitzsimmons J N, et al. 2019. Dissolved cadmium and cadmium stable isotopes in the western Arctic Ocean. Geochimica et Cosmochimica Acta, 258: 258–273, doi: 10.1016/j.gca.2019.05.028

Zhang Ruifeng, John S G, Zhang Jing, et al. 2015a. Transport and reaction of iron and iron stable isotopes in glacial meltwaters on Svalbard near Kongsfjorden: from rivers to estuary to ocean. Earth and Planetary Science Letters, 424: 201–211, doi: 10.1016/j.epsl.2015.05.031

Zhang Ruifeng, Ren Jingling, Zhang Zhuoyi, et al. 2022. Distribution patterns of dissolved trace metals (Fe, Ni, Cu, Zn, Cd, and Pb) in China marginal seas during the GEOTRACES GP06-CN cruise. Chemical Geology, 604: 120948, doi: 10.1016/j.chemgeo.2022.120948

Zhang Ruifeng, Zhang Jing, Ren Jingling, et al. 2015b. X-Vane: a sampling assembly combining a Niskin-X bottle and titanium frame vane for trace metal analysis of sea water. Marine Chemistry, 177: 653–661, doi: 10.1016/j.marchem.2015.10.006

Zhao Ye, Vance D, Abouchami W, et al. 2014. Biogeochemical cycling of zinc and its isotopes in the Southern Ocean. Geochimica et Cosmochimica Acta, 125: 653–672, doi: 10.1016/j.gca.2013.07.045